HHS Public Access

Author manuscript

ACS Appl Mater Interfaces. Author manuscript; available in PMC 2023 December 04.

Coating Bioactive Microcapsules with Tannic Acid Enhances the Phenotype of the Encapsulated Pluripotent Stem Cells

Daheui Choi,
Department of Physiology and Biomedical Engineering, Mayo Clinic, Rochester, Minnesota 55905, United States

Kihak Gwon,
Department of Physiology and Biomedical Engineering, Mayo Clinic, Rochester, Minnesota 55905, United States

Hye Jin Hong,
Department of Physiology and Biomedical Engineering, Mayo Clinic, Rochester, Minnesota 55905, United States

Harihara Baskaran,
Department of Chemical and Biomolecular Engineering, Case Western Reserve University, Cleveland, Ohio 44106, United States

Olalla Calvo-Lozano,
Nanobiosensors and Bioanalytical Applications Group (NanoB2A), Catalan Institute of Nanoscience and Nanotechnology (ICN2), CSIC, CIBERBBN and BIST, Barcelona 08193, Spain

Alan M. Gonzalez-Suarez,
Department of Physiology and Biomedical Engineering, Mayo Clinic, Rochester, Minnesota 55905, United States

Kyungtae Park,
Department of Chemical and Biomolecular Engineering, Yonsei University, Seoul 03722, Republic of Korea

Jose M. de Hoyos-Vega,
Department of Physiology and Biomedical Engineering, Mayo Clinic, Rochester, Minnesota 55905, United States

Corresponding Author Alexander Revzin – Department of Physiology and Biomedical Engineering, Mayo Clinic, Rochester, Minnesota 55905, United States; revzin.alexander@mayo.edu.

Author Contributions

D.C., K.G., H.J.H., and J.M.d. H.-V. performed the experiments. H. B. carried out the model experiment for capsule permeability. A.M. G.-S. designed and developed the encapsulation microfluidic devices. K.P. and J.H. measured AFM. O.C.-L. and L.M.L. carried out SPR analysis. G.S. and A.R. analyzed the data and supervised article description. All authors have given approval to the final version of the article.

The authors declare no competing financial interest.

Supporting Information

The Supporting Information is available free of charge at https://pubs.acs.org/doi/10.1021/acsami.2c06783.

Schematic illustration and images of the encapsulation device, thickness reduction graph according to TA film degradation, SPR analysis for the bFGF binding study, live/dead staining images of encapsulated H9 cells, visualization of TA on Hep capsules, and appendix for MATLAB code (PDF)

Laura M. Lechuga,
Nanobiosensors and Bioanalytical Applications Group (NanoB2A), Catalan Institute of Nanoscience and Nanotechnology (ICN2), CSIC, CIBERBBN and BIST, Barcelona 08193, Spain

Jinkee Hong,
Department of Chemical and Biomolecular Engineering, Yonsei University, Seoul 03722, Republic of Korea

Gulnaz Stybayeva,
Department of Physiology and Biomedical Engineering, Mayo Clinic, Rochester, Minnesota 55905, United States

Alexander Revzin
Department of Physiology and Biomedical Engineering, Mayo Clinic, Rochester, Minnesota 55905, United States

Abstract

Human pluripotent stem cells (hPSCs) may be differentiated into any adult cell type and therefore hold incredible promise for cell therapeutics and disease modeling. There is increasing interest in three-dimensional (3D) hPSC culture because of improved differentiation outcomes and potential for scale up. Our team has recently described bioactive heparin (Hep)-containing core–shell microcapsules that promote rapid aggregation of stem cells into spheroids and may also be loaded with growth factors for the local and sustained delivery to the encapsulated cells. In this study, we explored the possibility of further modulating bioactivity of microcapsules through the use of an ultrathin coating composed of tannic acid (TA). Deposition of the TA film onto model substrates functionalized with Hep and poly(ethylene glycol) was characterized by ellipsometry and atomic force microscopy. Furthermore, the presence of the TA coating was observed to increase the amount of basic fibroblast growth factor (bFGF) incorporation by up to twofold and to extend its release from 5 to 7 days. Most significantly, TA-microcapsules loaded with bFGF induced higher levels of pluripotency expression compared to uncoated microcapsules containing bFGF. Engineered microcapsules described here represent a new stem cell culture approach that enables 3D cultivation and relies on local delivery of inductive cues.

Graphical Abstract

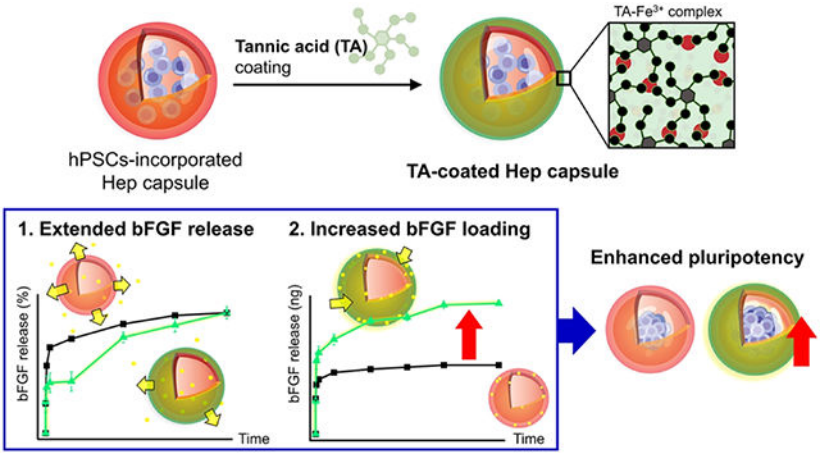

Keywords

microfluidics; heparin-based microcapsules; tannic acid; nanofilm; controlled growth factor release; 3D stem cell cultures

1. INTRODUCTION

Human pluripotent stem cells (hPSCs) are capable of unlimited proliferation and may be differentiated into any adult cell type.[1,2] Because of these properties, hPSCs hold incredible potential as a source of adult cells for cellular therapies, tissue engineering, and disease modeling.[3-5] Increasingly, the stem cell biology community has recognized both biological (e.g., improved differentiation outcomes) and practical benefits (e.g., scale up) of cultivating hPSCs in a 3D format.[6-9] 3D culture formats recently reported in the literature include hanging drop,[10,11] scaffold-based 3D culture,[12] as well as spheroid cultures under stirring or rocking conditions.[13-16] Despite these published reports, there remains a need for efficient and cost-effective differentiation protocols.

Microcapsules represent an interesting format for encapsulation and cultivation of stem cells.[17-20] Several reports described maintenance of pluripotency and proliferation of stem cells inside alginate hydrogel microbeads.[21,22] More recent reports focused on directed differentiation of encapsulated PSCs. For example, Finklea et al. demonstrated the use of PEG-fibrinogen microspheres for encapsulation of PSCs and differentiation of cardiomyocytes.[23] He et al. developed microcapsules composed of an alginate shell and a hyaluronic acid-enriched core and also demonstrated high-efficiency cardiac differentiation of PSCs.[24] Our team has also been interested in the use of core–shell microcapsules for the cultivation and differentiation of PSCs. Previously, we demonstrated that microcapsules with a PEG hydrogel shell and an aqueous core may be used to (1) promote aggregation of encapsulated stem cells into spheroids and (2) protect encapsulated spheroids against mechanical agitation in a stirred bioreactor.[25] Most recently, we described bioactive Hep-containing core–shell microcapsules that may be loaded with growth factors (GFs) for local and sustained delivery of inductive cues to the encapsulated hPSC spheroids.[26]

In the present study, we sought to further modulate physicochemical and biological properties of microcapsules through the use of an ultrathin coating (see Scheme 1). There have been a number of reports describing ultrathin coating approaches for stem cell cultivation and differentiation.[27-31] Multilayer films of polyelectrolytes such as heparin or chondroitin sulfate have been used to control the loading and release of GFs for proliferation and differentiation of stem cells.[27] In another approach, nanofilm coatings composed of vitronectin or fibronectin were used to mimic ECM–cell interactions and improve cultivation of iPSCs.[30,31] We should point out that the abovementioned studies were concerned with direct deposition of ultrathin coatings on cells, and to the best of our knowledge, there have not been reports describing ultrathin coatings applied to microcapsules carrying stem cells.

We chose to employ tannic acid (TA), a polyphenol derivative composed of gallic acid linked to a glucose core, because of its biocompatibility and ease of deposition.[32,33] The presence of phenyl groups in the TA structure promotes hydrogen bonding and hydrophobic interactions with proteins.[34,35] We hypothesized that an ultrathin coating may be used to further modulate bioactivity of our heparin-containing microcapsules.

We first characterized film assembly, thickness, and surface morphology on a model planar substrate (silicon) and then proceeded to coat microcapsules. Subsequently, we characterized effects of TA coating on permeability and GF loading/release properties of heparin-based microcapsules. Finally, we demonstrated that the presence of the TA coating improved the pluripotency expression of encapsulated hPSC spheroids.

2. MATERIALS AND METHODS

2.1. Materials.

Sodium heparin was purchased from Smithfield BioScience (Cincinnati, OH, USA). Methacrylic anhydride (MA), absolute ethanol, 1-ethyl-3-(3-dimethylaminopropyl) carbodiimide, cysteamine, dithiothreitol (DTT), 35 kDa PEG, triethanolamine (TEA), mineral oil, Span-80, iron(III) chloride hexahydrate ($FeCl_3 \cdot 6H_2O$), TA, deferiprone (DFP), fluorescein isothiocyanate (FITC), and bovine serum albumin (BSA) were purchased from Sigma-Aldrich (St. Louis, MO, USA). A 3.5 kDa Mw cut-off (MWCO) dialysis bag was purchased from Spectrum Laboratories (Rancho Dominguez, CA, USA). 1-Hydroxybenzotriazole hydrate was from AnaSpec Inc (Fremont, CA, USA). 10 kDa four-arm PEG-maleimide (PEG4MAL) was purchased from Laysan Inc (Arab, AL, USA). We followed previously published protocols to synthesize heparin–methacrylate (Hep–MA)[26] and heparin–thiol (Hep–SH).[36,37]

Passage 3 mouse embryonic fibroblasts (MEFs) (EmbryoMaxR PMEF P3, Strain CF-1, Untreated) were purchased from MilliporeSigma (Burlington, MA, USA). Dulbecco's modified Eagle medium (DMEM), ES-FBS, penicillin–streptomycin (P/S), DMEM/F12, Knockout Serum Replacer (KOSR), non-essential amino acids (NEAA), GlutaMAX, 2-mercaptoethanol, and TrypLE Express were purchased from Thermo Fisher Scientific (Waltham, MA, USA). AggreWell 400, Optiprep densifier, and mTeSR medium were from STEMCELL Technologies (Vancouver, Canada). The live/dead staining kit and donkey anti-mouse IgG secondary antibody-Alexa Fluor 546 were obtained from Invitrogen (Waltham,

MA, USA). The anti-SOX2 antibody, bFGF, and an ELISA kit for bFGF were purchased from R&D Systems (Minneapolis, MN, USA). DAPI was from Vector Lab (San Francisco, CA, USA). A 100 μm cell strainer was from Cardinal Health (Dublin, OH, USA). An RNA extraction kit (RNeasy kit) was obtained from Qiagen (Valencia, CA, USA). The OCT compound was purchased from Fisher Healthcare (Waltham, MA, USA).

2.2. Maintaining and Expanding PSCs.

We used the human embryonic stem cell line H9 in this study. H9 cells were maintained on an irradiated MEF feeder layer. P3 MEFs were cultured and expanded for two more passages (P5) in a medium based on DMEM with 10% ES-FBS, 1% P/S, and 2 mM GlutaMAX. The cells at passage 5 were trypsinized, collected in a 15 mL conical tube, and then irradiated at 20 Gy to mitotically inactivate them as feeder cells. The irradiated MEFs were cryopreserved at a concentration of 2×10^6 cells/vial for later use.

MEFs were seeded in a six-well plate with a concentration of 3×10^5 cells/well and cultured for 24 h. Afterward, the MEF media were removed, and H9 cells were seeded at a concentration of 2×10^4 cells/well. Pluripotency media (referred to as H9 media in the paper) were composed of DMEM/F12, 20% KOSR, 1× NEAA, 2 mM GlutaMAX, 0.1 mM 2-mercaptoethanol, and 100 ng/mL bFGF. Media (2 mL per well) were changed daily over the course of 5 days. Unencapsulated H9 spheroids were used as one of the controls for our study. These spheroids were created by seeding H9 cells into a commercial 3D culture plate (AggreWell). We previously determined that this cell concentration resulted in a seeding density of ~200 cells per well and produced spheroids that were comparable in dimensions (150 μm in diameter) to those observed inside microcapsules. H9 media (see above for composition) were used for cultivation of spheroids in AggreWell plates. Media were changed every other day.

2.3. Fabrication of Microfluidic Devices for Stem Cell Encapsulation.

We have previously described a microfluidic encapsulation system consisting of a filtration device located upstream of a flow-focusing capsule fabrication device.26 Detailed protocols for fabricating and operating this encapsulation system have been reported elsewhere.[26,38] Briefly, a co-axial flow-focusing device for cell encapsulation was fabricated by polydimethylsiloxane (PDMS) soft lithography. The device consisted of a total of four PDMS layers that were arranged into mirrored halves, each half with structures of three different heights. The mirrored PDMS slabs were treated with oxygen plasma and bonded to create a non-planar (3D) co-axial flow-focusing device. This device had channels of three heights: (1) 120 μm for the aqueous core channel, (2) 200 μm for aqueous shell channels, and (3) 300 μm for shielding oil, cross-linker oil, and capsule collection channels. The filtration microfluidic device consisted of a single 50 μm tall chamber populated with 200 μm triangle posts. The spacing between the posts varied from 400 μm at the inlet to 30 at the outlet.[16] This device was designed to trap cell aggregates and to ensure that single cells but not cell clusters enter the capsule fabrication device.

2.4. Operation of the Microfluidic Cell Encapsulation System.

Fabrication of core–shell microcapsules proceeded as follows. The co-axial flow-focusing microfluidic device was loaded with four different solutions: (1) core solution with 8% (w/v) PEG (35 kDa) and 17% (v/v) Optiprep densifier; (2) shell solution with 4% (w/v) Hep–MA, 8% (w/v) PEG4MAL (10 kDa), and 15 mM TEA; (3) shielding oil with mineral oil and 0.5% Span-80; and (4) a cross-linking emulsifier with 60 mM DTT dispersed in mineral oil with 3% Span-80. Each of the four solutions was filtered through 0.2 μm filters and loaded into syringes under sterile conditions and infused into separate inlets of a microfluidic device using syringe pumps (Harvard Apparatus) at the following rates: core (4 μL/min), shell (4 μL/min), shielding oil (50 μL/min), and cross-linking oil (60 μL/min). Microcapsules were then collected into a 15 mL in volume Falcon tube containing 1% BSA in 1× phosphate buffered saline (PBS) and incubated at 37 °C for 30 min. The capsules resided in the oil phase layer above the aqueous layer in the tube and slowly partitioned into the liquid phase. The mineral oil in the tube was aspirated, and microcapsules were harvested using a 100 μm cell strainer.

For cell encapsulation experiments, H9 cells were digested using TrypLE Express and re-suspended in the core solution at a concentration of 5×10^7 cells/mL. Flow rates of the core, shell, shielding oil, and cross-linker oil streams were maintained at 4, 4, 50, and 60 μL/min, respectively. A cell suspension solution was first passed through the filter device and injected into the encapsulation device.[26] The H9 encapsulated microcapsules were collected into a 15 mL tube filled with 5 mL of mTeSR medium, then distributed into a six-well plate, and incubated at 37 °C with 5% CO_2.

2.5. Tannic Acid–Fe^{3+} Film (TA Film) Coating.

2.5.1. TA Film Formation on Planar Substrates.—We wanted to first use planar substrates to deposit and characterize TA films.[39,40] Si wafers sputter-coated with a 100 nm Au layer (10 mm × 10 mm) and surface plasmon resonance (SPR) chips (Biosensing Instruments) were cleaned by first immersing in isopropanol for 30 min while ultra-sonicating and then exposed to oxygen plasma for 3 min. Subsequently, the substrates were immersed in a 1:2 mixture of Hep–thiol (0.5 mg/mL in 1× PBS) and PEG–thiol (1 mg/mL in 1× PBS) and kept overnight at 25 °C in the dark. The substrates were rinsed three times with 1× PBS and dried in air. To deposit the TA film, substrates containing a Hep–PEG layer were placed into a 5 mL centrifuge tube, and 2.4 mL of DI water was added. Then, 0.3 mL of both TA and $FeCl_3 \cdot 6H_2O$ solutions were sequentially added to adjust final concentrations of TA and $FeCl_3 \cdot 6H_2O$ in the solution to 0.4 and 0.1 mg/mL, respectively. To change the pH to around 7, 1 M NaOH solution was added. The solution in the tube was vigorously agitated for 10 s to form the TA layer. Then, the gold substrate was washed with 1× PBS three times to remove unbound TA and $FeCl_3 \cdot 6H_2O$. The film preparation process was repeated until the desired number of layers was formed.

2.5.2. Coating on Hep Microcapsules with TA Film.—The protocol for depositing a TA film onto microcapsules was similar to the coating of a planar substrate. Briefly, 2000 Hep microcapsules were placed in 2.4 mL of DI water in a 15 mL conical tube. Subsequently, 0.3 mL of TA (0.1 mg/mL) was added first, followed by 0.3 mL

of $FeCl_3 \cdot 6H_2O$ (0.1 mg/mL). We followed a previously reported protocol for TA film formation.[39] Briefly, interactions between TA and Fe^{3+} ions resulted in a product that changed the solution color to purple. Once this color change was observed, the solution pH was adjusted to 7 by adding 4 μL of 1 M NaOH. This was done in order to improve the efficiency of the polymerization reaction. The mixture was agitated by gentle pipetting for 10 s. Then, the Hep microcapsules were collected using a 100 μm strainer to remove the residual solution and were washed with 1× PBS 5–7 times while on the strainer to remove unbound TA and $FeCl_3 \cdot 6H_2O$. The process was repeated in the exact same way to add new TA layers.

2.5.3. Depositing TA Film in Monolayer Cultures of hPSCs.—We envisioned the possibility of TA deposits not only on microcapsules but also on encapsulated cells and wanted to assess whether such direct deposition of TA has positive or negative effects on viability and pluripotency of H9 cells. For this experiment, 1×10^5 cells/well of H9 cells were seeded on a six-well plate and maintained in H9 pluripotency media for one day. Subsequently, media were aspirated, and cells were exposed to 0.1 mg/mL of TA and $FeCl_3 \cdot 6H_2O$ in 1× PBS. Then, 1 M of NaOH was added to adjust the pH to neutral, and the solution was agitated for 10 s. The solution was removed and washed with 1× PBS five times. The H9 cells were cultured in H9 media for 5 days and analyzed by RT-PCR for expression of pluripotency markers.

2.6. Characterization of TA Coating.

2.6.1. Quantification of Thickness, Surface Topography, and the Amount of TA Deposited onto Model Planar Substrates and on Microcapsules.—Film thickness and surface topography of the TA film on a flat substrate were measured by ellipsometry (LSE-USB, Gaertner Scientific) and atomic force microscopy (AFM; NX-10, Park Systems), respectively. To quantify the amount of deposited TA, Hep–PEG-grafted Au substrates were prepared to contain three TA layers. Then, the substrates were immersed in 1–50 mM of DFP aqueous solution at 37 °C for 3 days. Degradation of the film was assessed by making ellipsometry measurements at different time points.

The amount of TA deposited on microcapsules was quantified by UV–vis spectroscopy (NanoDrop One-C; Thermo Fisher Scientific) as follows. Batches of 10,000 Hep capsules were coated with 1, 3, or 5 layers of TA as described before. Subsequently, capsules were immersed in 1 mM DFP solution at 37 °C for 3 days to degrade the TA film solution. The solution containing the disassembled TA film was analyzed by UV–vis absorption. Because absorption spectra of DFP and TA overlapped in the 200–290 nm wavelength range, we only considered absorption peaks at 300 nm for quantitation of TA. Calibration curves were constructed by measuring absorbance values for TA concentrations ranging from 0 to 125 μg/mL, TA concentrations from unknown samples were then determined using these calibration curves.

2.6.2. SPR Analysis of bFGF Binding to Model Surfaces.—Au-coated SPR chips were functionalized with the Hep–PEG or Hep–PEG/TA film as described in Section 2.5.1. A solution of bFGF in 1× PBS (100 ng/mL, 120 μL) was injected into the flow cell of

an SPR instrument at a flow rate of 20 μL/min. Binding studies were carried out using SPR from Biosensing Instruments with control and data analysis software (Biosensing Instruments Inc).

2.6.3. Microscopy Characterization of TA Film Formation on Microcapsules.

—TA layer adsorption onto microcapsules was characterized by fluorescence microscopy following a strategy described in the literature.[39] This strategy entailed first labeling BSA with isothiocyanate in FITC using a standard protocol. Then, TA-coated microcapsules were incubated in 1 mg/mL of BSA-FITC in 1× PBS for 30 min at 37 °C. A similar protocol was used to visualize the presence of the TA film atop 2D cultures of H9 cells. After incubation with BSA-FITC and prior to fluorescence imaging, capsules or cell cultures were washed three times with 1× PBS. Microscopy was carried out using standard fluorescence (IX83, Olympus) and confocal microscopes (LSM 780, Zeiss).

2.6.4. Assessing Permeability of the Hep Microcapsule with and without the TA Film.—

To quantify permeability, 2000 microcapsules were loaded with FITC-dextran (1 μM in 1× PBS, either 20, 70, or 2000 kDa) for 3 h at 37 °C. Subsequently, microcapsules were quickly transferred into pristine 1× PBS solution and mounted onto a microscope (IX83, Olympus) to characterize release of fluorescent dextran. Images of microcapsules were analyzed using ImageJ. The same protocol was carried out for microcapsules carrying 0, 1, or 3 layers of TA.

2.6.5. Estimating Permeability and Diffusivity of TA-Coated Microcapsules Using Modeling.—

Diffusivity values were estimated using a custom-developed function in MATLAB (MathWorks). The function estimates permeability (m/s) of the dextran molecule across the microcapsule from the experimental intensity data normalized to the initial ($t = 0$) intensity. The MATLAB function pdepe was used to solve the dimensionless form of the unsteady diffusional transport equation and associated boundary and initial conditions

$$\frac{\partial C'}{\partial t'} = \frac{1}{r'^2}\frac{\partial}{\partial r'}\left(r'^2\frac{\partial C'}{\partial r'}\right)$$

Initial condition: $\mathrm{at}\, t' = 0, C' = 1$

Boundary conditions: $\mathrm{at}\, r' = 0,\ \partial C' / \partial r' = 0,\ \mathrm{at}\, r' = 1,\ \partial C' / \partial r' = -\alpha C'$

Here, $C' = C / C_0$, $r' = r / R$, $t' = tD / R^2$, $\alpha = PR / D$, R is the radius of the microcapsule (200 μm), C_0 is the initial intensity, D is the diffusivity of the dextran in the aqueous core (44, 33, and 0.9 $\mu m^2/s$ for 20, 70, and 2000 kDa dextran, respectively), and P is the permeability of the dextran molecule in the shell. For an initial guess of the permeability value, the solution of the above equation yielded normalized concentration values as a function of the dimensionless radial position and at experimental time points. Concentration versus radial position data were integrated across the sphere and averaged to obtain mean intensity values versus time from the model. These were compared to experimental data at various time points, and an objective function was established using summed square values of the

error between the experimental data and the model estimate. The objective function was minimized using the MATLAB function fmincon using α as a parameter to yield an optimal value of dextran permeability across the shell. The MATLAB code is illustrated in the Appendix in detail.

2.7. Loading and Release of bFGF.

We tested two different protocols for coating the TA film and loading bFGF in Hep microcapsules. The “coat-then-load” protocol involved depositing the TA film first and loading bFGF second. This sequence was reversed for the “load-then-coat” protocol.

For the “load-then-coat” protocol, 2000 Hep microcapsules were placed into 2 mL of 100 ng/mL bFGF solution in 1× PBS for 3 h at 37 °C. Then, the microcapsules were collected using a 100 μm strainer and coated with either 1 or 3 layers of TA as described above. To establish a rigorous control for microcapsules without TA, we imitated the coating protocol (washing, pipetting, etc.) but did not include TA–Fe reagents in the solution. The “coat-then-load” protocol was carried out by first depositing 1 or 3 layers of TA onto microcapsules and then immersing microcapsules in the bFGF solution as described above.

To assess the release of bFGF, 2000 microcapsules were placed on a 100 μm strainer inside 2 mL of 1× PBS in a well of a six-well plate. Capsules were moved into fresh solution of 1× PBS at specific points in time, and the residual solution was analyzed for bFGF using ELISA and a microplate reader (Synergy H1, BioTek).

We also fluorescently labeled bFGF to visualize GF incorporation into microcapsules. Labeling bFGF with FITC was carried out using a standard protocol.[41] Loading of bFGF-FITC into microcapsules was accomplished according to the protocol described in the paragraph above. After loading, Hep microcapsules were moved to pristine 1× PBS and were imaged using a fluorescence microscope.

2.8. Depositing the TA Film onto Hep Microcapsules with Stem Cells and Assessing Pluripotency.

After encapsulation, H9 cells were maintained in pluripotency media (mTeSR) for 1 day to promote spheroid formation. Then, Hep microcapsules were transferred into H9 media for 24 h to load bFGF. Deposition of the TA layer was carried out as described above (Section 2.5.2 TA film coating on Hep microcapsules). TA-coated or bare microcapsules were separated into two groups based on the mode of bFGF presentation and were cultured for an additional 4 days. In one group, capsules were cultured in H9 media supplemented with bFGF. This group was called “soluble” throughout the paper. The other group of microcapsules was cultured in H9 media without bFGF. This group was called “immobilized” because encapsulated stem cells only experienced bFGF that was loaded at the beginning of the 5 day experiment. The same experimental groups were created for microcapsules that were first loaded with bFGF and then coated with TA.

2.9. Viability and Proliferation of Encapsulated H9 Cells.

H9 cell viability was assessed using the live/dead assay, where live and dead cells emitted green and red fluorescence, respectively. The live/dead staining was carried out following the manufacturer's protocol. Cells were imaged using a fluorescence microscope and quantified with ImageJ software.

We used H9 cells to quantify cell proliferation in microcapsules. The bright-field cellular images were acquired 1, 3, and 5 days after encapsulation. The spheroid size was assessed using ImageJ software.

2.10. Assessment of Pluripotency with RT-PCR and Immunofluorescence.

To examine levels of pluripotency gene expression, 2000 microcapsules containing hPSC spheroids were broken up by applying an electronic pestle for 5 min in the cell lysis buffer. Then, total RNA was extracted using a commercial kit following the manufacturer's instructions. Approximately 50–60 ng of total extracted RNA was used for synthesis of cDNA, following the reverse transcription kit protocol (Roche). The primer sequences used for RT-PCR are listed in Table S1. Gene expression was verified using the QuantStudioTM 5 System (Thermo Fisher Scientific) with SYBR Green and was normalized to glyceraldehyde 3-phosphate dehydrogenase. The amplification procedure for real-time PCR consists of 40 cycles of denaturation at 95 °C for 5 s, annealing at 55 °C for 15 s, and extension at 69 °C for 20 s. The final analysis was performed based on the threshold cycles using the ΔΔCT method.

For immunofluorescence staining, encapsulated or bare spheroids were fixed with 4% paraformaldehyde for 1 h and subsequently immersed in 30% v/v sucrose solution in 1× PBS for 24 h. Before cryo-sectioning, the spheroids were imbedded in the OCT compound. The samples were sectioned into 10 μm thick slices using a cryostat (Leica CM1950) and placed on a glass slide. The sectioned spheroids were then permeabilized by immersing in 0.1% Triton X-100 in 1× PBS solution for 20 min and blocked with 2% BSA–PBS for 1.5 h at 25 °C. Then, the slides were incubated with primary Ab—5 μg/mL of anti-Sox2 Abs in 1× PBS and 1% w/v of BSA. Then, the slides were immersed in the solution of secondary Ab—2 μg/mL of donkey anti-mouse IgG and secondary antibody-Alexa Fluor 546—and were treated for 1 h in the dark to conjugate to primary antibodies. Finally, 50 μL of mounting medium containing DAPI was dispensed onto sectioned spheroids and placed under a coverslip (170 μm; Fisher Healthcare). Imaging was assessed using an Olympus fluorescence microscope.

2.11. Statistical Analysis.

All experiments were performed at least in three replications. To verify the significance of each group in the case of more than three groups, one-way ANOVA analysis followed by Tukey's post hoc was evaluated. For comparison significance between the two groups, a paired Student's *t*-test for control and experimental data was evaluated. The significance was denoted as *, **, ***, and NS, which means $p < 0.05$, $p < 0.01$, $p < 0.001$, and non-significant, respectively.

3. RESULTS AND DISCUSSION

3.1. Characterization of the TA Film.

Our team has an interest in developing microcapsules with a PEG–Hep shell and an aqueous core that may be loaded with GFs for local and continuous delivery to the encapsulated stem cells.[26] In this paper, we wanted to test a hypothesis that coating a microcapsule with an ultrathin film may further enhance the phenotype of the encapsulated stem cells by either slowing down the diffusion or improving the retention of GFs. To form an ultrathin coating, we focused on TA—a polyphenol with a glucose core—that has been shown to rapidly assemble into structured thin films in the presence of metal ions such as Fe^{3+}.[39,40,42] TA molecules interact with Fe ions via coordination bonding and form stable films of defined thickness. TA is a common food additive present in green tea or wine and, therefore, has excellent biocompatibility.[43,44] We envisioned that a TA film would overcoat a microcapsule as shown in Figure 1A. However, before proceeding to microcapsule coating, we wanted to characterize properties of a TA film under better-controlled conditions using surface analysis approaches. For this purpose, gold-coated Si substrates were functionalized using a 2:1 solution mixture of PEG–thiol and Hep–thiol in order to approximate the stoichiometry of PEG and Hep molecules in the hydrogel shell. The PEG–thiol and Hep–thiol molecules assembled and formed a 2.5 nm layer on the substrate as measured by ellipsometry. A subsequent step of incubating a substrate in a solution containing TA and Fe^{3+} molecules resulted in deposition of a 6.5 nm layer (see Figure 1B). Interestingly, a similar thickness increase was observed when depositing the second and third layers of TA. Thus, ellipsometry analysis revealed that TA films could be formed on a substrate containing a Hep–PEG layer and that multiple TA layers could be assembled sequentially. Additional characterization of substrates was performed by AFM. As shown in Figure 1C, deposition of the TA film resulted in the appearance of sparsely dispersed 30–40 nm clusters. The presence of similar clusters has been reported previously and may represent non-uniformity in film formation or presence of TA–Fe^{3+} nucleation sites.[45-47] The deposition of three layers of the TA film produced substrates with a much denser distribution of the clusters. The surface roughness (R_q) increased from 4.108 to 6.682 nm for 1- and 3-layer TA films, respectively. Thus, AFM analysis confirmed the deposition of TA films onto the PEG–Hep layer and pointed to expansion of nucleation sites as a possible film growth mechanism.[48]

In the next set of experiments, we characterized deposition of the TA film on Hep microcapsules. The microcapsules are fabricated using a flow-focusing microfluidic device as described in our previous publications and in Figure S1. Co-axial core and shell flow streams are ejected into the oil stream, forming droplets. These droplets are then polymerized in situ in the microfluidic device by reaction of a dithiol cross-linker (DTT) with PEG4MAL molecules present in the shell. The core contains non-reactive high MW PEG molecules that leach out and are displaced by water molecules. The result is the formation of microcapsules with a hydrogel shell (~10–15, μm) and an aqueous core.[26] These microcapsules are incubated in the solution containing TA and Fe^{3+} to create an ultrathin film. Because TA interacts with proteins via hydrogen bonding or hydrophobic interactions,[49] we used BSA-FITC to visualize the presence of the thin film. As seen from Figure 1D, BSA-FITC molecules interacted with TA-coated microcapsules but not

with bare microcapsules. Confocal microscopy revealed that the fluorescence signal was localized to the perimeter of a capsule, forming ~2.84 and 6.81 μm annulus for 1- and 3-layer TA coatings, respectively. These observations pointed to the depth of penetration of TA molecules into and TA–Fe network growth inside the hydrogel—a behavior that was fundamentally different from that of planar substrates.

As the next step, we quantified the amount of TA deposited onto microcapsules as a function of layer number. To achieve this, we first used TA-coated Si substrates and ellipsometry measurements to establish the concentration of the iron chelator (DFP) and incubation time that led to complete dissociation of the TA film (see Figure S2). Then, these optimal conditions were used to dissociate the TA coating from microcapsules. The concentration of TA in the solution was established with spectrophotometry using a calibration curve (see Figure S3). This experiment revealed that deposition of 1, 3, or 5 layers resulted in 3.79, 4.33, and 5.31 ng of TA per capsule, respectively (Figure 1E). Unlike a solid substrate where film thickness (and the amount of deposited material) scaled linearly with the number of layers, the amount of TA adsorbed onto microcapsules increased only moderately and non-linearly with the number of layers. This may be explained by the different mode of film formation in the hydrogel that likely occurred along the polymeric segments and around water-retaining pores.

3.2. Assessing Diffusivity of Hep Microcapsules after Deposition of TA Film.

Fluorescence imaging of FITC-dextran was used to assess diffusivity of microcapsules as a function of TA film deposition. In this experiment, microcapsules were first loaded by incubating with FITC-dextran (20, 70, or 2000 kDa) and then transferred to pristine PBS solution to observe changes in fluorescence of microcapsules during release. In-capsule fluorescence was monitored and plotted over time to create release curves of the type shown in Figure 2A,C,E. These data were also fitted to an unsteady-state diffusional transport equation to estimate diffusivity and permeability of the hydrogel shell for dextrans of different MWs.

The results of this experiment are compiled in Figure 2 and may be used to draw several observations. First, as shown in Figure 2A, the presence of one layer of TA resulted in a modest (~1.4-fold) decrease in diffusivity for 20 kDa dextran when compared to bare capsules. A three-layer TA coating had a 2.6-fold lower diffusivity compared to that of bare capsules. For both coating types, complete release occurred after 2 h (Figure 2B). Given that 20 kDa of dextran approximates the size of bFGF, this observation suggests that TA coating was not expected to slow down diffusion of bFGF enough to affect a multi-day stem cell culture experiment.

In contrast, 70 and 2000 kDa dextrans diffused more slowly from overcoated microcapsules, with 40–60% of fluorescence retained in such microcapsules at a 30 min time point (Figure 2C-F). Only 20–30% of fluorescence was observed in bare microcapsules at the same time point. It is also worth noting that residual in-capsule fluorescence was only observed at a 2 h timepoint for 2000 kDa dextran release from microcapsules containing three layers of TA. This suggests once again that TA coating does not appreciably impede diffusion of molecules on the size scale of large proteins. Given that hydrodynamic radii of 20, 70,

and 2000 kDa dextrans are ~4, ~6, and 27 nm respectively,[50] we estimate the pore size for microcapsules without TA coating and with one layer of TA film to be >30 nm. In the case of a three-layer TA coating, the pore size may be in the 10–30 nm range.

3.3. Effects of TA Coating on Loading and Release of bFGF.

Our goal is to use bioactive microcapsules for cultivation of PSCs. bFGF is the key inductive signal in most pluripotency maintenance protocols.[51] We have previously shown that Hep microcapsules retain and release bFGF in a controlled manner over the course of 5 days.[26] In this paper, we wanted to assess the effects of the TA film on release of bFGF from Hep microcapsules. We explored two modes of bFGF incorporation into overcoated microcapsules. (1) The "load-then-coat" method, with microcapsules first incubated in 100 ng/mL of bFGF solution for loading and then coated with the TA film. For this loading protocol, we had an additional experimental group called bare + coating that was designed to simulate rigorous washing involved in TA coating and to account for the potential loss of bFGF during such washing. We note that bFGF was loaded, but the film was not deposited on capsules for the bare + coating experimental group. (2) The other protocol explored here was "coat-then-load," with microcapsules first coated by TA and then loaded with bFGF.

Given that 1 and 3 layers were shown to result in a similar amount of TA incorporation into microcapsules as well as in similar diffusion properties for 20 and 70 kDa dextrans that best approximated the size of GFs, henceforth, we focused on one-layer TA coating. After loading bFGF, microcapsules were transferred into pristine PBS solution and maintained for 7–10 days with daily solution changes. ELISA was used to quantify (1) the amount of bFGF loaded after initial incubation and (2) release of bFGF over time. Figure 3 summarizes outcomes for this set of experiments. Looking at the "load-then-coat" method for incorporating bFGF and TA into microcapsules (see Figure 3A-C), it may be noted that the presence of TA coating resulted in a much slower release of bFGF compared to bare microcapsules. On day 2, only 45% of bFGF was released from coated capsules compared to 80% from bare capsules. It is also worth noting that the amount of bFGF loaded into coated and bare microcapsules was similar, which is 19 and 17 ng, respectively (per 2000 capsules). The other scenario explored here was "coat-then-load," where the TA film was first formed on microcapsules and bFGF was loaded as a second step. The experimental results for this scenario are described in Figure 3D-F. It may be noted that differences in release profiles for this scenario were not as dramatic as those described for "load-then-coat" microcapsules. After 2 days, ~75 and 85% of bFGF were released from coated and bare microcapsules, respectively. However, it was interesting to observe that the amount of loaded bFGF was twofold higher for coated microcapsules compared to that of bare microcapsules (~40 vs ~21 ng per 2000 capsules). This suggests that, in the coated microcapsules, Hep binding sites are supplemented with TA moieties, resulting in greater capacity for uptake of bFGF. This observation is consistent with reports describing avid interactions of GFs with TA coating via hydrogen bonding and hydrophobic interactions.[52,53]

We went back to the model substrates to carry out SPR analysis and confirm bFGF deposition onto chemical layers resembling those comprising microcapsules. This analysis (see Figure S4 and Table S2) revealed that the TA layer deposited atop the Hep–PEG layer

adsorbed ~three times more bFGF compared to the Hep–PEG layer alone. SPR analysis on model substrates in combination with ELISA for microcapsules confirms that the presence of TA coating enhances loading of bFGF.

Our experiments underscore differences in loading and release of bFGF for the “load-then-coat” versus “coat-then-load” modes of microcapsule preparation. For the former, the release appears to be slower, likely because bFGF molecules imbedded in the Hep hydrogel are diffusing through and binding to the TA layer on the way out. For the latter mode of capsule preparation, bFGF molecules localize at the TA/water interface and are released more rapidly; however, the loading capacity for bFGF is increased by a factor of 2.

Taking dextran diffusion studies together with loading and release of bFGF, we conclude that TA coating does not appreciably affect diffusivity of a microcapsule but does enhance its capacity for binding bFGF. Thus, TA–GF affinity interactions governed slower release of bFGF from overcoated microcapsules observed in Figure 3A,C.

3.4. Assessing the Effects of a TA Coating on Viability and Proliferative Capacity of the Encapsulated PSCs.

Having characterized the effects of TA coating on loading and release of bFGF from microcapsules, we proceeded to investigate its effects on viability and proliferative capacity of hPSCs. Feeder-dependent H9 cells were used for these experiments. H9 cells were encapsulated with a flow-focusing device as described in Figure S1 using an input concentration of 50×10^6 cells/mL. A typical encapsulation run produced 400 μm diameter microcapsules with 90% cell occupancy,[25] 200 cells per capsule and viability >90% (see Figures 4A,B and S5). Encapsulated H9 cells were placed into mTeSR media for 24 h and began to aggregate within that timeframe. TA coating was applied 1 day after encapsulation, and then microcapsules were switched to H9 pluripotency media (containing bFGF) and cultured for a total of 5 days. As seen from a panel of images in Figure 4C, spheroids proliferated rapidly inside microcapsules. Importantly, TA coating had no discernible effects on viability (Figure 4B) or proliferative capacity of H9 cells (Figure 4C,D). The results described in this section support the notion of TA coating being non-toxic to and compatible with the encapsulated hPSCs.

3.5. Evaluating Pluripotency of the Encapsulated hPSCs.

As the final step in our study, we wanted to evaluate how pluripotency maintenance of H9 cells is affected by encapsulation, TA coating, and immobilization of bFGF. We have recently published a study that described encapsulation of feeder-independent HUES-8 cells adapted for 3D cultures.[25,26] This past study demonstrated that Hep microcapsules loaded with bFGF and TGF-β1 supported the pluripotent phenotype of HUES-8 cells. Importantly, inductive cues were loaded once and then released locally to the encapsulated cells over the course of 5 days. The present study not only focuses on further enhancing bioactivity of microcapsules but also uses an H9 cell line that is feeder dependent. We proceeded to characterize the pluripotency of encapsulated stem cells, benchmarking them against standard cultures on feeders as well as against H9 spheroid cultures without capsules. Thus,

we wanted to discern whether differences in pluripotency were due to bioactivity of the microcapsule or the culture format (2D vs 3D).

Is it possible that TA film deposits directly on the encapsulated stem cells and, if so, may it have a positive effect on cell phenotype expression? To answer this question, we first investigated the presence of TA moieties on the encapsulated cells. As before, BSA-FITC was employed for visualization of TA coating. As shown in Figure S6, we did indeed see co-localization of green fluorescence with encapsulated cells, suggesting that TA molecules were deposited onto cells. As the next step, we wanted to account for the possibility that TA had a direct positive effect on stem cell pluripotency, for example, by binding and localizing bFGF atop cells. We, therefore, created another control culture condition with H9 cells cultured on feeders and overcoated with the TA film. This condition was denoted as 2D w/TA.

As discussed in the preceding section, we studied two scenarios for loading microcapsules with bFGF and coating with TA—"load-then-coat" and "coat-then-load". When compared with uncoated microcapsules, the former scenario was associated with slower release, while the latter resulted in twofold higher incorporation of bFGF. Here, we assessed pluripotency gene expression and carried out immunofluorescence staining for both types of microcapsules. In addition, we also compared the effects of one-time loading of bFGF into microcapsules and subsequent cultivation without bFGF in the media (denoted with superscript Imm), to exposure of encapsulated stem cells to soluble bFGF with daily media exchanges (denoted by superscript Sol).

Figure 5A summarizes RT-PCR analysis of three pluripotency genes for the "load-then-coat" microcapsules. The first observation is that the three control groups without Hep gel (2D, 2D w/TA, and spheroid) had similar levels of pluripotency gene expression after 5 days of culture in H9 pluripotency media complete with 100 ng/mL bFGF. This means that (1) TA coating deposited directly onto H9 cells did not improve their pluripotency and (2) the 3D spheroid format alone did not contribute to improved pluripotency. The second observation was that H9 cells in bare Hep microcapsules (w/o TA coating) expressed significantly better levels of pluripotency genes compared to controls. The reader may remember that we wanted to account for potential loss of bFGF due to rigorous washing that is part of the TA coating. Therefore, uncoated microcapsules were incubated with bFGF and then underwent a protocol that mimicked coating without depositing TA. This group was called bare + coating (C). For this group, one-time loading of bFGF induced similar levels of Sox2 and Oct4 expressions on day 5 of culture compared to daily exposure to soluble bFGF during this timeframe. The exception was the Nanog expression, where the bare + C^{Sol} condition was significantly better than bare + C^{Imm}. A third observation was that TA coating of microcapsules resulted in a moderate but significant increase in pluripotency gene expression compared to uncoated or bare microcapsules. Pluripotency was confirmed using immunofluorescence staining and is shown in Figures 5B and S7.

Figure 5C summarizes the pluripotency gene expression for "coat-then-load" microcapsules. Similar to the discussion above, H9 cells in Hep microcapsules expressed much better pluripotency compared to standard culture conditions (both 2D and 3D). Here,

microcapsules coated with TA and exposed to soluble bFGF in pluripotency media (TA^{Sol}) induced significantly better expression of pluripotent genes compared to uncoated microcapsules or coated microcapsules loaded with bFGF without further supplementation of this signal in the media (TA^{Imm}). For the TA^{Sol} condition, Oct4 was 3.94-fold and Nanog was 1.58-fold higher compared to the $Bare^{Imm}$ experimental group. While Sox2 gene expression was not significantly different between TA^{Sol} and $Bare^{Imm}$ conditions, immunofluorescence staining and subsequent quantitation revealed higher levels of Sox2 staining in TA^{Sol} microcapsules compared to $Bare^{Imm}$ and TA^{Imm} conditions (see Figures 5D and S7).

The results described in Figure 5 are exciting for multiple reasons. First, we highlight that H9 cells cultured in bioactive microcapsules in the absence of feeder cells express pluripotency genes at a much higher level than in standard cultures on feeders. This suggests that a higher level of pluripotency signaling in Hep microcapsules nullifies the need for feeders, at least for this particular cell line. We also highlight the fact that bioactive Hep-containing microcapsules may be loaded with inductive cues for sustained release to the encapsulated stem cells. Such a culture format may obviate the need for daily supplementation of soluble bFGF and may make cultivation of hPSC more affordable.

Finally, we demonstrate that the presence of TA coating on Hep microcapsules further enhances their bioactivity. Here, coated microcapsules loaded with bFGF (immobilized condition) induced significantly better pluripotency gene expression compared to bare microcapsules with either immobilized or soluble bFGF. We should note, however, that the best pluripotency gene expression was observed for “coat-then-load” microcapsules exposed to soluble bFGF. The reader may recall that such capsules had a twofold better loading capacity for bFGF compared to standard Hep microcapsules. We therefore surmise that the ability to sustain a high local concentration of bFGF in these microcapsules translates into improved pluripotency.

4. CONCLUSIONS

This study focused on ultrathin TA coating for modulating bioactivity of Hep-containing microcapsules. We first characterized TA film formation on model solid substrates and then explored coating of hydrogel microcapsules. This comparison revealed that while the amount of TA scaled linearly with the number of layers on a solid substrate, it increased only moderately on hydrogel microcapsules. We also noted that the TA film/network was formed not as an outer layer at the hydrogel shell–aqueous interface but within the hydrogel shell. While this remains to be proven experimentally, it is likely that TA deposition occurred along the polymer chains and around the water-filled pores of the hydrogel. TA coating was associated with only a modest decrease in diffusivity across the hydrogel shell of microcapsules, as confirmed with fluorescent dextrans. The TA coating did, however, have pronounced effects on increased loading and extended release of bFGF—an inductive cue commonly used for maintenance of hPSCs. Depending on the TA coating format, bFGF release could be extended from 5 to 7 days, or its loading amount could be increased by a factor of 2 compared to uncoated Hep microcapsules. The improved loading and release characteristics of coated microcapsules are attributable to affinity interactions

between TA moieties and bFGF molecules. Importantly, TA-coated microcapsules induced better expression of pluripotency markers in the encapsulated H9 cells. To the best of our knowledge, this is the first description of an ultrathin coating used to improve bioactivity of microcapsules and maintenance of encapsulated PSCs. Moving forward, we will leverage TA-coated microcapsules to carry out directed differentiation along pancreatic and hepatic lineages.

Supplementary Material

Refer to Web version on PubMed Central for supplementary material.

ACKNOWLEDGMENTS

This study was supported in part by the grants from the Mayo Clinic Center for Regenerative Medicine, J.W. Kieckhefer Foundation, Al Nahyan Foundation, Regenerative Medicine Minnesota (RMM 101617 TR 004), and NIH (DK107255). Additional support was provided by an NIH Grant EB021911 to H.B. Additional funding was provided by the Mayo Clinic Center for Cell Signaling in Gastroenterology (P30DK084567).

REFERENCES

(1). Pera MF; Reubinoff B; Trounson A Human Embryonic Stem Cells. J. Cell Sci 2000, 113, 5–10. [PubMed: 10591620]

(2). McDevitt TC; Palecek SP Innovation in the Culture and Derivation of Pluripotent Human Stem Cells. Curr. Opin. Biotechnol 2008, 19, 527–533. [PubMed: 18760357]

(3). Gepstein L. Derivation and Potential Applications of Human Embryonic Stem Cells. Circ. Res 2002, 91, 866–876. [PubMed: 12433831]

(4). Stojkovic M; Lako M; Strachan T; Murdoch A Derivation, Growth and Applications of Human Embryonic Stem Cells. Reproduction 2004, 128, 259–267. [PubMed: 15333777]

(5). Martín M; Menéndez P Biological Impact of Human Embryonic Stem Cells. Stem Cell Transplantation; Springer, 2012; pp 217–230.

(6). Preynat-Seauve O; Suter DM; Tirefort D; Turchi L; Virolle T; Chneiweiss H; Foti M; Lobrinus JA; Stoppini L; Feki A Development of Human Nervous Tissue upon Differentiation of Embryonic Stem Cells in Three-Dimensional Culture. Stem Cells 2009, 27, 509. [PubMed: 19074418]

(7). Mohr JC; de Pablo JJ; Palecek SP 3-D Microwell Culture of Human Embryonic Stem Cells. Biomaterials 2006, 27, 6032–6042. [PubMed: 16884768]

(8). Lei Y; Jeong D; Xiao J; Schaffer DV Developing Defined and Scalable 3D Culture Systems for Culturing Human Pluripotent Stem Cells at High Densities. Cell. Mol. Bioeng 2014, 7, 172–183. [PubMed: 25419247]

(9). Chaicharoenaudomrung N; Kunhorm P; Noisa P Three-Dimensional Cell Culture Systems as an in vitro Platform for Cancer and Stem Cell Modeling. World J. Stem Cell 2019, 11, 1065.

(10). Cerdan C; Hong SH; Bhatia M Formation and Hematopoietic Differentiation of Human Embryoid Bodies by Suspension and Hanging Drop Cultures. Curr. Protoc. Stem Cell Biol 2007, 3, Unit 1D.2.1.

(11). Yoon BS; Yoo SJ; Lee JE; You S; Lee HT; Yoon HS Enhanced Differentiation of Human Embryonic Stem Cells into Cardiomyocytes by Combining Hanging Drop Culture and 5-Azacytidine Treatment. Differentiation 2006, 74, 149–159. [PubMed: 16683985]

(12). Smith LA; Liu X; Hu J; Ma PX The Enhancement of Human Embryonic Stem Cell Osteogenic Differentiation with Nano-Fibrous Scaffolding. Biomaterials 2010, 31, 5526–5535. [PubMed: 20430439]

(13). Rohani L; Borys BS; Razian G; Naghsh P; Liu S; Johnson AA; Machiraju P; Holland H; Lewis IA; Groves RA; Toms D; Gordon PMK; Li JW; So T; Dang T; Kallos MS; Rancourt DE Stirred Suspension Bioreactors Maintain Naïve Pluripotency of Human Pluripotent Stem Cells. Commun. Biol 2020, 3, 492. [PubMed: 32895477]

(14). Lam AT-L; Li J; Toh JP-W; Sim EJ-H; Chen AK-L; Chan JK-Y; Choolani M; Reuveny S; Birch WR; Oh SK-W Biodegradable Poly-ε-Caprolactone Microcarriers for Efficient Production of Human Mesenchymal Stromal Cells and Secreted Cytokines in Batch and Fed-Batch Bioreactors. Cytotherapy 2017, 19, 419–432. [PubMed: 28017598]

(15). Ting S; Chen A; Reuveny S; Oh S An Intermittent Rocking Platform for Integrated Expansion and Differentiation of Human Pluripotent Stem Cells to Cardiomyocytes in Suspended Microcarrier Cultures. Stem Cell Res. 2014, 13, 202–213. [PubMed: 25043964]

(16). Borys BS; So T; Colter J; Dang T; Roberts EL; Revay T; Larijani L; Krawetz R; Lewis I; Argiropoulos B; Rancourt DE; Jung S; Hashimura Y; Lee B; Kallos MS Optimized Serial Expansion of Human Induced Pluripotent Stem Cells using Low-Density Inoculation to Generate Clinically Relevant Quantities in Vertical-Wheel Bioreactors. Stem Cells Transl. Med 2020, 9, 1036–1052. [PubMed: 32445290]

(17). Zhao S; Xu Z; Wang H; Reese BE; Gushchina LV; Jiang M; Agarwal P; Xu J; Zhang M; Shen R Bioengineering of Injectable Encapsulated Aggregates of Pluripotent Stem Cells for Therapy of Myocardial Infarction. Nat. Commun 2016, 7, 13306. [PubMed: 27786170]

(18). Zhang W; Zhao S; Rao W; Snyder J; Choi JK; Wang J; Khan IA; Saleh NB; Mohler PJ; Yu J; Hund TJ; Tang C; He X A Novel Core–Shell Microcapsule for Encapsulation and 3D Culture of Embryonic Stem Cells. J. Mater. Chem. B 2013, 1, 1002–1009.

(19). Choe G; Kim S-W; Park J; Park J; Kim S; Kim YS; Ahn Y; Jung D-W; Williams DR; Lee JY Anti-Oxidant Activity Reinforced Reduced Graphene Oxide/Alginate Microgels: Mesen-chymal Stem Cell Encapsulation and Regeneration of Infarcted Hearts. Biomaterials 2019, 225, 119513. [PubMed: 31569016]

(20). Siti-Ismail N; Bishop AE; Polak JM; Mantalaris A The Benefit of Human Embryonic Stem Cell Encapsulation for Prolonged Feeder-Free Maintenance. Biomaterials 2008, 29, 3946–3952. [PubMed: 18639332]

(21). Serra M; Correia C; Malpique R; Brito C; Jensen J; Bjorquist P; Carrondo MJT; Alves PM Microencapsulation Technology: a Powerful Tool for Integrating Expansion and Cryopreservation of Human Embryonic Stem Cells. PLoS One 2011, 6, No. e23212. [PubMed: 21850261]

(22). Choe G; Park J; Park H; Lee J Hydrogel Biomaterials for Stem Cell Microencapsulation. Polymers 2018, 10, 997. [PubMed: 30960922]

(23). Finklea FB; Tian Y; Kerscher P; Seeto WJ; Ellis ME; Lipke EA Engineered Cardiac Tissue Microsphere Production through Direct Differentiation of Hydrogel-Encapsulated Human Pluripotent Stem Cells. Biomaterials 2021, 274, 120818. [PubMed: 34023620]

(24). Xu J; Shamul JG; Staten NA; White AM; Jiang B; He X Bioinspired 3D Culture in Nanoliter Hyaluronic Acid-Rich Core–Shell Hydrogel Microcapsules Isolates Highly Pluripotent Human iPSCs. Small 2021, 17, 2102219.

(25). Fattahi P; Rahimian A; Slama MQ; Gwon K; Gonzalez-Suarez AM; Wolf J; Baskaran H; Duffy CD; Stybayeva G; Peterson QP; Revzin A Core–Shell Hydrogel Microcapsules Enable Formation of Human Pluripotent Stem Cell Spheroids and Their Cultivation in a Stirred Bioreactor. Sci. Rep 2021, 11, 7177. [PubMed: 33785778]

(26). Gwon K; Hong HJ; Gonzalez-Suarez AM; Slama MQ; Choi D; Hong J; Baskaran H; Stybayeva G; Peterson QP; Revzin A Bioactive Hydrogel Microcapsules for Guiding Stem Cell Fate Decisions by Release and Reloading of Growth Factors. Bioact. Mater 2022, 15, 1–14. [PubMed: 35386345]

(27). Macdonald ML; Samuel RE; Shah NJ; Padera RF; Beben YM; Hammond PT Tissue Integration of Growth Factor-Eluting Layer-By-Layer Polyelectrolyte Multilayer Coated Implants. Biomaterials 2011, 32, 1446–1453. [PubMed: 21084117]

(28). Min J; Braatz RD; Hammond PT Tunable Staged Release of Therapeutics from Layer-By-Layer Coatings with Clay Interlayer Barrier. Biomaterials 2014, 35, 2507–2517. [PubMed: 24388389]

(29). Damanik FFR; Brunelli M; Pastorino L; Ruggiero C; Van Blitterswijk C; Rotmans J; Moroni L Sustained Delivery of Growth Factors with High Loading Efficiency in a Layer By Layer Assembly. Biomater. Sci 2020, 8, 174–188.

(30). Han U; Kim YJ; Kim W; Park JH; Hong J Construction of Nano-Scale Cellular Environments by Coating a Multilayer Nanofilm on the Surface of Human Induced Pluripotent Stem Cells. Nanoscale 2019, 11, 13541–13551. [PubMed: 31290516]

(31). Han U; Kim W; Cha H; Park JH; Hong J Nano-Structure of Vitronectin/Heparin on Cell Membrane for Stimulating Single Cell in iPSC-Derived Embryoid Body. Iscience 2021, 24, 102297. [PubMed: 33851104]

(32). Abouelmagd SA; Abd Ellah NH; Amen O; Abdelmoez A; Mohamed NG Self-Assembled Tannic Acid Complexes for pH-Responsive Delivery of Antibiotics: Role of Drug-Carrier Interactions. Int. J. Pharm 2019, 562, 76–85. [PubMed: 30851388]

(33). Mori T; Rezai-Zadeh K; Koyama N; Arendash GW; Yamaguchi H; Kakuda N; Horikoshi-Sakuraba Y; Tan J; Town T Tannic acid is a Natural β-Secretase Inhibitor that Prevents Cognitive Impairment and Mitigates Alzheimer-Like Pathology in Transgenic Mice. J. Biol. Chem 2012, 287, 6912–6927. [PubMed: 22219198]

(34). Hagerman AE Chemistry of Tannin-Protein Complexation. Chemistry and Significance of Condensed Tannins; Springer, 1989; pp 323–333.

(35). Lee H; Dellatore SM; Miller WM; Messersmith PB Mussel-Inspired Surface Chemistry for Multifunctional Coatings. science 2007, 318, 426–430. [PubMed: 17947576]

(36). Tae G; Kim Y-J; Choi W-I; Kim M; Stayton PS; Hoffman AS Formation of a Novel Heparin-Based Hydrogel in the Presence of Heparin-Binding Biomolecules. Biomacromolecules 2007, 8, 1979–1986. [PubMed: 17511500]

(37). Gwon K; Kim E; Tae G Heparin-Hyaluronic Acid Hydrogel in Support of Cellular Activities of 3D Encapsulated Adipose Derived Stem Cells. Acta Biomater. 2017, 49, 284–295. [PubMed: 27919839]

(38). Gwon K; Hong HJ; Gonzalez-Suarez AM; Stybayeva G; Revzin A Microfluidic Fabrication of Core-Shell Microcapsules carrying Human Pluripotent Stem Cell Spheroids. J. Visualized Exp 2021, 176, No. e62944.

(39). Ejima H; Richardson JJ; Liang K; Best JP; van Koeverden MP; Such GK; Cui J; Caruso F One-Step Assembly of Coordination Complexes for Versatile Film and Particle Engineering. Science 2013, 341, 154–157. [PubMed: 23846899]

(40). Lee J; Cho H; Choi J; Kim D; Hong D; Park JH; Yang SH; Choi IS Chemical Sporulation and Germination: Cytoprotective Nanocoating of Individual Mammalian Cells with a Degradable Tannic Acid–Fe III Complex. Nanoscale 2015, 7, 18918–18922. [PubMed: 26528931]

(41). Choi GH; Lee HJ; Lee SC Titanium-A dhesive Polymer Nanoparticles as a Surface-R eleasing System of Dual Osteogenic Growth Factors. Macromol. Biosci 2014, 14, 496–507. [PubMed: 24227631]

(42). Yun G; Richardson JJ; Capelli M; Hu Y; Besford QA; Weiss ACG; Lee H; Choi IS; Gibson BC; Reineck P; Caruso F The Biomolecular Corona in 2D and Reverse: Patterning Metal–Phenolic Networks on Proteins, Lpids, Ncleic Aids, Plysaccharides, and Fngerprints. Adv. Funct. Mater 2020, 30, 1905805.

(43). Turgut Coşan D; Saydam F; Özbayer C; Doğaner F; Soyocak A; Güneş HV; Değirmenci İ; Kurt H; Üstüner MC; Bal C Impact of Tannic Acid on Blood Pressure, Oxidative Stress and Urinary Parameters in L-NNA-Induced Hypertensive Rats. Cytotechnology 2015, 67, 97–105. [PubMed: 24306272]

(44). Wang Y; Liu S; Ding K; Zhang Y; Ding X; Mi J Quaternary Tannic Acid with Improved Leachability and Biocompat-ibility for Antibacterial Medical Thermoplastic Polyurethane Catheters. J. Mater. Chem. B 2021, 9, 4746–4762. [PubMed: 34095937]

(45). Huang Y; Lin Q; Yu Y; Yu W Functionalization of Wood Fibers based on Immobilization of Tannic Acid and in situ Complexation of Fe (II) Ions. Appl Surf. Sci 2020, 510, 145436.

(46). Li D; Shen H; Cai C; Sun T; Zhao Y; Chen L; Zhao N; Xu J Fabrication of Conductive Silver Microtubes using Natural Catkin as a Template. ACS Omega 2017, 2, 1738–1745. [PubMed: 31457537]

(47). Rahim MA; Ejima H; Cho KL; Kempe K; Müllner M; Best JP; Caruso F Coordination-Driven Multistep Assembly of Metal–Polyphenol Films and Capsules. Chem. Mater 2014, 26, 1645–1653.

(48). Lee H; Nguyen DT; Kim N; Han SY; Hong YJ; Yun G; Kim BJ; Choi IS Enzyme-Mediated Kinetic Control of Fe3+–Tannic Acid Complexation for Interface Engineering. ACS Appl. Mater. Interfaces 2021, 13, 52385–52394.

(49). Choi D; Heo J; Hong J Controllable drug release from nano-layered hollow carrier by non-human enzyme. Nanoscale 2018, 10, 18228–18237. [PubMed: 30232482]

(50). Pilz M; Kwapiszewska K; Kalwarczyk T; Bubak G; Nowis D; Hońyst R Transport of Nanoprobes in Multicellular Spheroids. Nanoscale 2020, 12, 19880–19887. [PubMed: 32975267]

(51). Mossahebi-Mohammadi M; Quan M; Zhang J-S; Li X FGF Signaling Pathway: a Key Regulator of Stem Cell Pluripotency. Front. Cell Dev. Biol 2020, 8, 79. [PubMed: 32133359]

(52). Choi D; Komeda M; Heo J; Hong J; Matsusaki M; Akashi M Vascular Endothelial Growth Factor Incorporated Multilayer Film Induces Preangiogenesis in Endothelial Cells. ACS Biomater. Sci. Eng 2018, 4, 1833–1842. [PubMed: 33445338]

(53). Shin M; Lee H-A; Lee M; Shin Y; Song J-J; Kang S-W; Nam D-H; Jeon EJ; Cho M; Do M; Park S; Lee MS; Jang J-H; Cho S-W; Kim K-S; Lee H Targeting Protein and Peptide Therapeutics to the Heart via Tannic Acid Modification. Nat. Biomed. Eng 2018, 2, 304–317. [PubMed: 30936449]

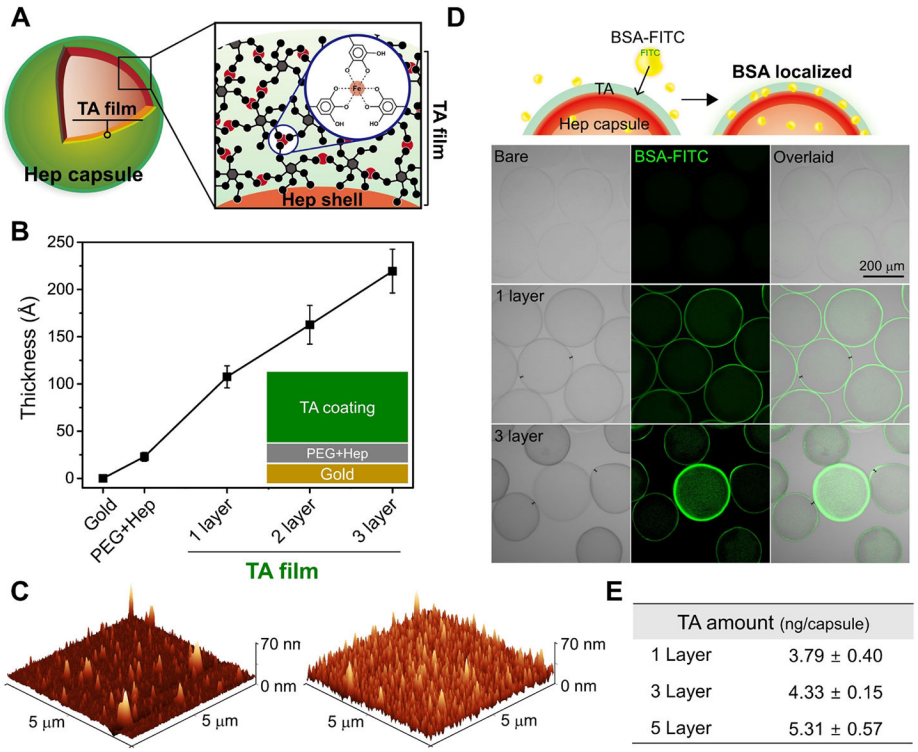

Figure 1.

Characterization of TA film formation on model substrates and on microcapsules. (A) Chemistry of the TA film with a close-up view of the coordination complexes between TA and Fe ions. (B) Ellipsometry analysis of changes in thickness due to the deposition of multiple TA layers onto a model gold substrate containing the PEG–SH/Hep–SH layer. (C) AFM analysis of topography for 1- and 3-layer TA coatings. (D) Microcapsules coated with different numbers of TA layers were incubated in BSA-FITC and characterized by microscopy to visualize localization of the TA film. (E) Microcapsules coated with TA layers were exposed to the Fe chelator to disassemble the film. The amount of TA removed from microcapsules was quantified using UV–vis.

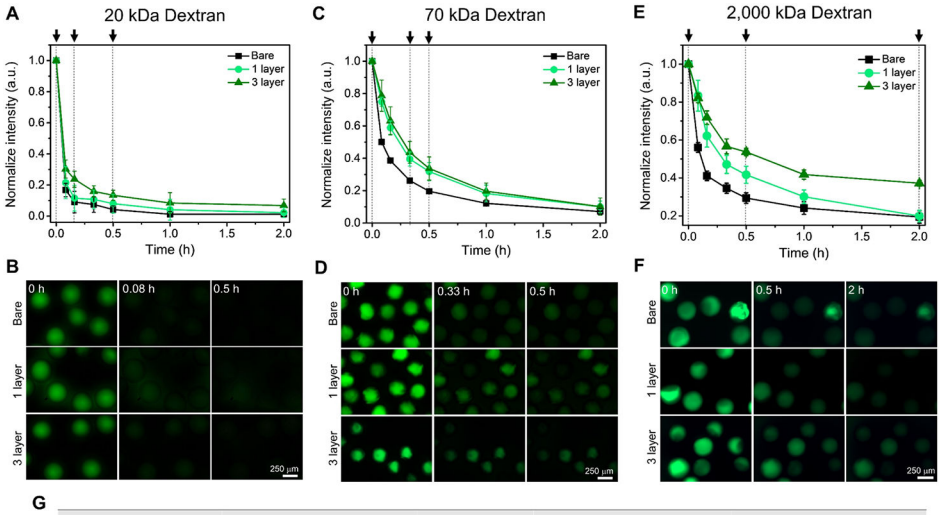

G

MW of dextran [kDa]	Diffusivity in Core [m²/s]	Type	Permeability [m/s]	Diffusivity in Shell [m²/s]
20	44×10^{-12}	Bare	7.94×10^{-7}	12.5×10^{-12}
		1 Layer	5.75×10^{-7}	9.07×10^{-12}
		3 Layer	3.01×10^{-7}	4.75×10^{-12}
70	33×10^{-12}	Bare	12.5×10^{-8}	19.8×10^{-13}
		1 Layer	5.38×10^{-8}	8.49×10^{-13}
		3 Layer	4.70×10^{-8}	7.41×10^{-13}
2,000	90×10^{-13}	Bare	19.9×10^{-8}	31.3×10^{-13}
		1 Layer	4.76×10^{-8}	7.51×10^{-13}
		3 Layer	2.23×10^{-8}	3.52×10^{-13}

Figure 2.

Diffusivity of TA-coated microcapsules assessed using FITC-dextrans. Capsules were loaded with FITC-dextran and then moved to pristine solution to monitor the decrease of in-capsule fluorescence over time. (A) In-capsule fluorescence as a function of TA layer number for diffusion of 20 kDa FITC-dextran. (B) Fluorescence images of microcapsules that correspond to black arrows in part A. (C) In-capsule fluorescence as a function of TA layer number for diffusion of 70 kDa FITC-dextran. (D) Fluorescence images of microcapsules that correspond to black arrows in part C. (E) In-capsule fluorescence analysis as a function of time for 2000 kDa FITC-dextran. (F) Fluorescence images that correspond to time points identified with black arrows in part E. (G) Experimental results from parts A, C, and E were fitted to a diffusion model setup in MATLAB to determine permeability and diffusivity values.

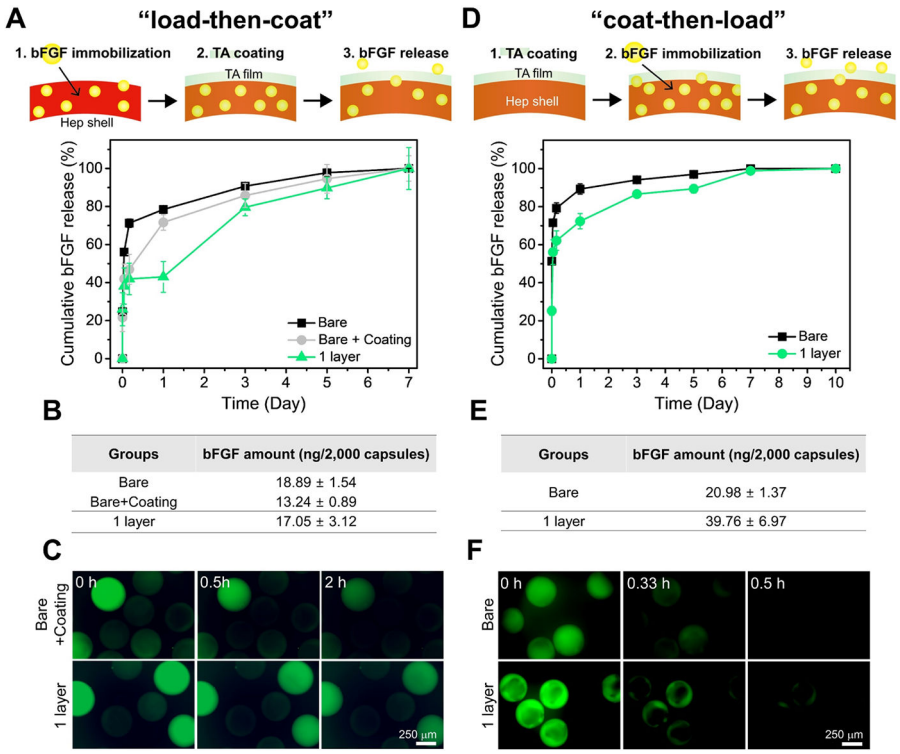

Figure 3.

Loading and release of bFGF from TA-coated microcapsules. (A) Microcapsules were first loaded with bFGF and then coated with the TA film. Solution bathing microcapsules were sampled daily and analyzed by ELISA to establish cumulative release of bFGF. Microcapsules in the bare + control group were exposed to rigorous washing associated with coating but did not receive TA coating. This was done to account for the possibility of GF release due to washing. (B) ELISA was used to determine the amount of bFGF loaded into microcapsules. (C) Use of FITC-labeled bFGF to confirm retention and release of this GF for "load-then-coat" microcapsules. (D) Different modes of the ultrathin film assembly and GF loading where capsules were first overcoated with TA and then loaded with bFGF. ELISA was used to determine bFGF release from microcapsules. (E) Results of ELISA analysis of the bFGF loading into "coat-then-load" microcapsules. (F) Visualizing retention and release from "coat-then-load" microcapsules using FITC-labeled bFGF. Description of experimental groups: "load-then-coat"—load bFGF into capsules and then coat with TA; bare—bare Hep microcapsules; bare + coating—bare Hep microcapsules with only the coating process in the absence of TA; (1) layer—1-layer TA-coated on bare Hep microcapsules. "Coat-then-load"—coat the TA layer first and then load bFGF into capsules; bare—Hep microcapsules without TA coating; 1-layer—TA-coated on bare Hep microcapsules.

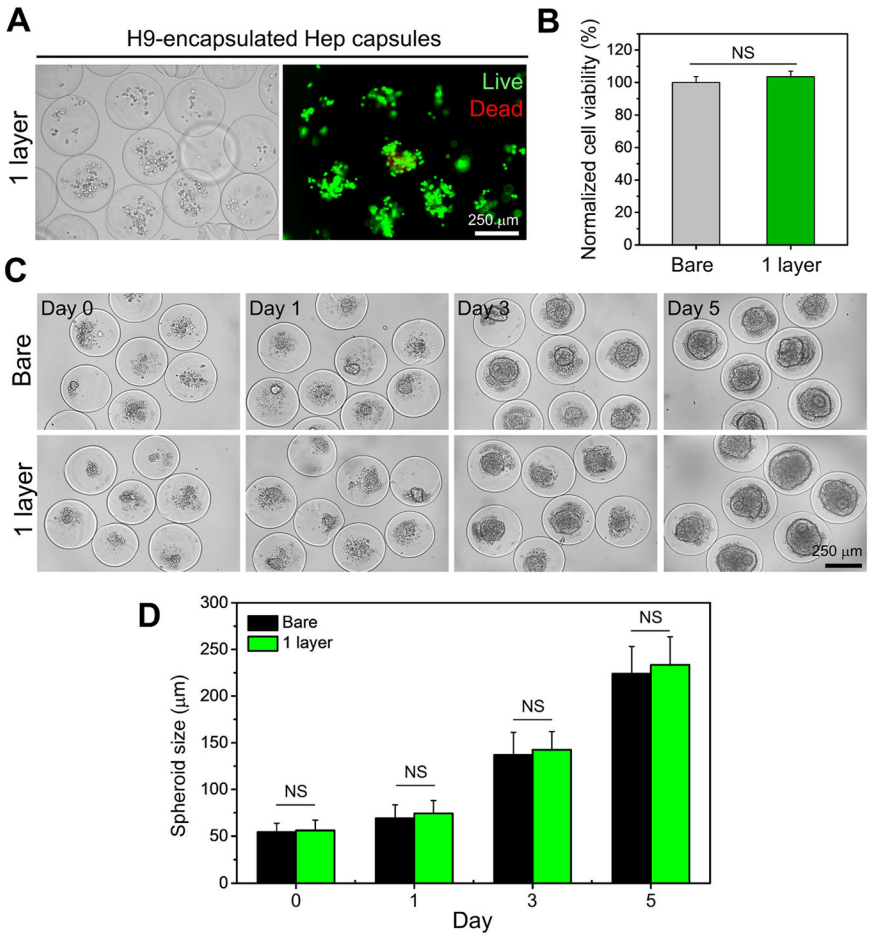

Figure 4.

Assessing viability and proliferative capacity of encapsulated stem cells. (A) Brightfield and fluorescence (live/dead) images of H9 cells ~2 h after encapsulation and TA coating. Cells were highly viable, as indicated by green fluorescence and little to no red fluorescence. (B) Viability of cells in 10 capsules was analyzed using ImageJ. No significant differences in viability were observed between bare and TA-coated microcapsules. (C) Brightfield images recording stem cell spheroid size change in bare and coated microcapsules. (D) Quantification of the spheroid diameter change based on 25 microcapsules revealed no significant difference between bare and TA-coated microcapsules. (NS, $p > 0.05$).

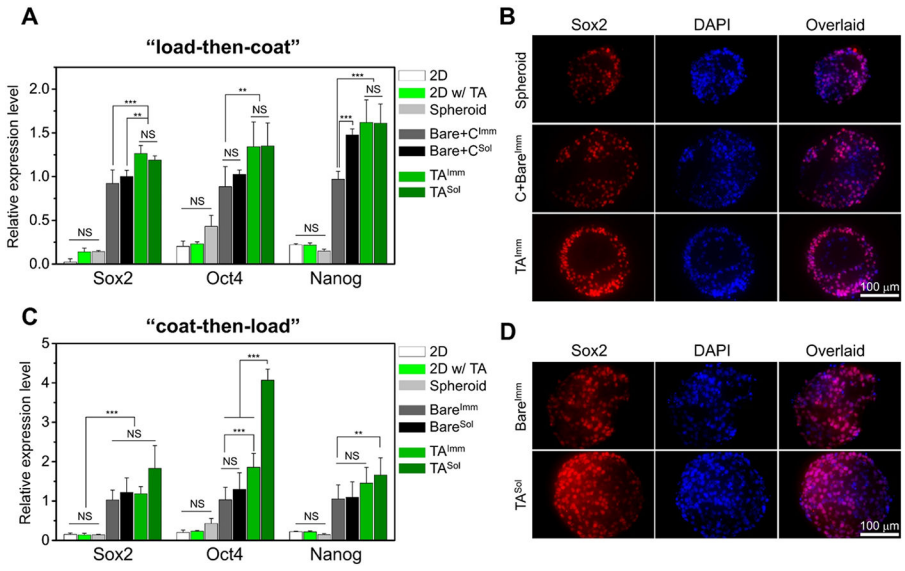

Figure 5.

Analysis of pluripotency of the encapsulated stem cells. (A) RT-PCR analysis of pluripotency gene expression for stem cells in microcapsules prepared by the "load-then-coat" method. Various experimental groups are described in greater detail below. (B) Immunofluorescence staining for Sox2 (red) and nuclei (blue, DAPI). (C) RT-PCR analysis of pluripotency gene expression for stem cells in microcapsules prepared by the "coat-then-load" method. (D) Immunofluorescence staining for pluripotency marker Sox2 for stem cells in "coat-then-load" microcapsules. Statistical analysis—number of samples = 4 (ns, $p > 0.05$; *, $p \leq 0.05$; **, $p \leq 0.01$; ***, $p \leq 0.001$). Description of experimental groups: 2D—standard H9 cultures on MEF in pluripotency media; 2D w/TA—as in previous but with TA coating; spheroid—H9 cell spheroids formed in 3D culture plates and maintained in pluripotency media; bare + C^{Imm}—encapsulated H9 cells that were exposed to rigorous washing without TA deposition; loaded with bFGF once and cultured without bFGF in the media; bare + C^{Sol}—as in previous but bFGF was present in the media during the experiment; TA^{Imm}—microcapsules loaded with bFGF, then overcoated with the TA film, and cultured without bFGF in the media; TA^{Sol}—as in previous but with bFGF present in the media throughout the experiment.

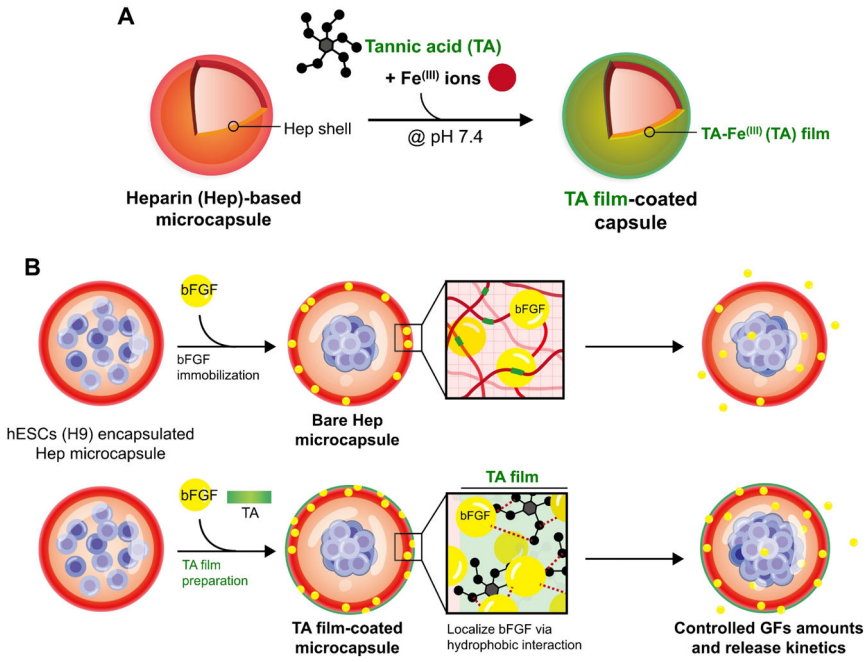

Scheme 1. Schematic Illustrating Ultrathin Coating of Stem Cell-containing Microcapsules [a]

[a] (A) TA molecules were cross-linked with Fe^{3+} ions to form a film atop and within a hydrogel microcapsule. (B) Microcapsules were composed of a Hep–PEG hydrogel shell and an aqueous core and carried PSCs. Properties of bare and coated microcapsules were compared with respect to loading/release of bFGF (an inductive cue) as well as pluripotency maintenance of the encapsulated stem cells.